Gradient-driven diffusion and pattern formation in crowded mixtures

Prithviraj Nandigrami, Brandy Grove, Andrew Konya, and Robin L. B. Selinger

Phys. Rev. E **95**, 022107 — Published 6 February 2017

DOI: 10.1103/PhysRevE.95.022107

Gradient-driven diffusion and pattern formation in crowded mixtures

Prithviraj Nandigrami

Department of Physics, Kent State University

Brandy Grove

Department of Macromolecular Science and Engineering, Case Western Reserve University

Andrew Konya and Robin L. B. Selinger

Liquid Crystal Institute, Kent State University

(Dated: December 2, 2016)

Abstract

Gradient-driven diffusion in crowded, multicomponent mixtures is a topic of high interest because of its role in biological processes such as transport in cell membranes. In partially phase-separated solutions, gradient-driven diffusion affects microstructure, which in turn affects diffusivity; a key question is how this complex coupling controls both transport and pattern formation. To examine these mechanisms, we study a two-dimensional multi-component lattice gas model, where "tracer" molecules diffuse between a source and a sink separated by a solution of sticky "crowder" molecules that cluster to form dynamically evolving obstacles. In the high temperature limit, crowders and tracers are miscible and transport may be predicted analytically. At intermediate temperatures, crowders phase separate into clusters that drift toward the tracer sink. As a result, steady-state tracer diffusivity depends non-monotonically on both temperature and crowder density and we observe a variety of complex microstructures. In the low temperature limit, crowders rapidly aggregate to form obstacles that are kinetically arrested; if crowder density is near the percolation threshold, resulting tracer diffusivity shows scaling behavior with the same scaling exponent as the random resistor network model. Though highly idealized, this simple model reveals fundamental mechanisms governing coupled gradient-driven diffusion, phase separation, and microstructural evolution in crowded solutions.

INTRODUCTION

Diffusion, aggregation, and coarsening in multi-component mixtures leads to a rich variety of morphologies in complex fluids [1]. In crowded environments, diffusive transport under a driving force often gives rise to complex pattern formation including striped structures [2]. Molecular diffusion in a crowded mixture containing multiple components affects both chemical reaction kinetics and pattern formation [3, 4]. Diffusion in crowded environments often plays a key role in transport within cell membranes [5, 6], and in solutions and cells [7]. Brownian motion is often observed in cellular environments such as bacterial cytoplasm [8], and other crowded biological environments [9]. For large macromolecules, the dominant transport behavior in such environments is diffusive in nature [8, 10, 11].

In a multi-component mixture, diffusivity of each molecular species depends on the density of all components present, interaction energy, and microstructure, that is, pattern formation during phase separation. Thus, diffusive transport and microstructure co-evolve and are coupled in general. Many multi-component simulation studies consider randomly distributed immobile crowders (obstacles) while tracers are allowed to diffuse [12, 13]. Recent modelling efforts investigated the effect of obstacle size [14], and the effects of attractive or repulsive interactions between tracers and immobile crowders [15]. In this paper, we consider a system where both tracers and crowders are allowed to diffuse, and where crowders have attractive interactions and may undergo phase separation to form dynamically evolving mobile obstacles.

Diffusive transport in crowded environments has been extensively investigated using a diverse range of simulation techniques, analytic models, as well as experiments [16–36]. In the recent years, several distinct simulation models have given particular emphasis on modeling anomalous diffusion processes in crowded medium. Of these, on-lattice simulation models [12, 37–44] summarize the different regimes for anomalous diffusion and how the system evolves to the stationary state. Off-lattice simulation models also have been proposed to describe anomalous diffusion in crowded media via Brownian Dynamics [45] as well as by taking into account hydrodynamic interactions [46, 47]. The effect of mobile obstacles on Brownian diffusion was recently investigated by Berry and Chaté [48], demonstrating that the nature of obstacle diffusion determines whether tracer motion is diffusive or sub-diffusive. Recent simulation studies have investigated the effect of bimolecular chemical reactions in

confined environments in the presence of crowding species in solution [49]. The resulting reaction rate shows sensitive dependence on density of the crowding species. The effect of macromolecular crowding on the collapse of biopolymers has very recently been investigated and scaling laws have been proposed [50].

In this paper, we examine the coupling of multi-species diffusive transport, phase separation, and pattern formation using the multi-component lattice gas model in two dimensions. The driving force for diffusion is provided by an applied density gradient, with boundary conditions on the density of a "tracer" species at the two edges of the cell, rather than by a constant external driving force as in related models [2]. Tracers diffuse through a solvent with a prescribed density of "crowder" species. Our model demonstrates that the resulting tracer flux and crowder microstructure both depend sensitively on crowder density, interaction strength, and temperature. This model could describe, for example, recent experiments by Gericke and coworkers [51], where a composition gradient in a lipid membrane is maintained using microfluidic methods, and the resulting lipid composition profile changes when crowder proteins are introduced. While this highly idealized model presented in this paper does not take into account hydrodynamic effects or detailed molecular scale interactions, it reveals several key fundamental mechanisms by which microstructural evolution and diffusive transport may mutually interact.

MODEL

We perform Monte Carlo (MC) simulations of a two-dimensional lattice gas model with two diffusing species, "tracers", and "crowders". The system Hamiltonian is $H = \sum_{i,j} U\Big(s_i, s_j\Big)$, where the sum is over nearest neighbor pairs and $s_i = 1, 2, 3$ refer to vacancy, tracer, and crowder particle types, respectively. At most one particle may occupy each lattice site, and vacancies are reminiscent of background solvent. Crowders have attractive nearest neighbor interaction energy $U(3,3) = -J_{\rm int}$, and can thus undergo phase separation as a function of temperature and density. All other interactions are excluded volume only, with $U(1,1) = U(1,2) = U(1,3) = U(2,1) = U(2,2) = U(2,3) = U(3,1) = U(3,2) = 0$. Thus, tracers have no energetic preference to aggregate with each other or bond to crowders. The dimensionless parameter $k_{\rm B}T_{\rm s}/J_{\rm int}$ sets the energy scale in our model, where $J_{\rm int}$ and $k_{\rm B}T_{\rm s}$ are independent parameters. The simulation cell is a square lattice of dimension L

with periodic boundary conditions in the y-direction only. In the initial state, crowders are randomly distributed throughout the simulation cell with a density ρ_{C}. We impose a density gradient of the tracer species along the x-direction by introducing a tracer-emitting source along the left side of the cell and a tracer-absorbing sink along the right side; that is, we impose the boundary condition that tracer density $\rho_{\mathrm{T}} = 1$ at $x = 0$ and $\rho_{\mathrm{T}} = 0$ at $x = L$.

Both tracer and crowder species diffuse via nearest neighbor hops implemented via the Metropolis algorithm [52]. The particle hopping rule implemented in this model is analogous to a model of diffusive percolation for "blind ants" where particles hop by choosing a site from all neighboring sites [54]. Particles may only move into a neighboring site if it is vacant. Thus, if there are no vacancies present, the system arrests and no further diffusion can occur. As tracers emerge from the source and are absorbed in the sink, the number of tracers changes with time while the number of crowders remain constant. Simulations were run for system size $L = 100$ for at least 2×10^9 Monte Carlo steps, where each Monte Carlo step represents one attempted move per lattice site. Each simulation time step is defined as one attempted Monte Carlo move per lattice site. Such long simulations are necessary to allow the system to reach steady state, even for such relatively small system sizes. We perform ten discrete simulation runs for each point in the phase space defined by (ρ_{C}, T_{s}). Simulated ensemble for each point in the phase space is constructed by averaging over the last 10% data of each simulation to capture the steady state behavior.

We examine the interaction of diffusive transport and microstructural evolution in this model system. We assume Fick's law diffusion, where tracer flux (J) is calculated by counting the number of tracer particles annihilating at the sink per unit length and per unit time; Net tracer flux is computed by counting the rate of tracers annihilating at the sink per unit length per unit time. We define the net diffusivity of tracers as D_{net}, and define D_0 as the net diffusivity of tracers in the absence of crowders. The quantity D_{net}/D_0 is thus calculated as tracer flux (with crowders) normalized by the tracer flux in the absence of crowders.

Crowder particles represent a lattice gas and at low temperature they phase separate into clusters which gradually coarsen. The presence of tracer diffusion alters this microstructural evolution: crowders drift toward the sink and form clusters which may be compact, elongated in the direction of tracer flow, or flattened against the sink. Likewise, diffusive transport of tracers is strongly affected by clustering of crowders which represent sticky mobile obstacles.

In the high temperature limit, where crowder attractive interactions can be neglected,

tracer diffusivity as a function of crowder density can be calculated analytically as described below. The introduction of attractive interactions for the crowder species completely changes the system behavior. Even in this highly idealized model, the resulting tracer diffusivity cannot be described by a simple function of temperature and crowder density but shows several characteristic regimes. Several previous studies have focused on models of diffusion in which diffusivity is typically reported as a function of crowder density. In our system, we apply a gradient in tracer diffusivity, which in turn induces a gradient in crowder density. The resulting pattern formation process governs the transport of the two species. This simplified model thus demonstrates a complex mechanism governing gradient-driven transport in multicomponent mixtures.

RESULTS

Temporal evolution

Temporal evolution of the system is shown in Fig. 1 for scaled temperature $k_{\mathrm{B}}T_s/J_{\mathrm{int}} = 0.25$ at crowder density (ρ_{C}) values of 0.1, 0.2, and 0.5. Here, T_{s} is the simulation temperature. Movies showing the time evolution of all three systems may be viewed in the supplementary information [53].

Crowders, shown in red, initially aggregate to form clusters which coarsen, drift gradually toward the sink, and aggregate there, as shown in Fig. 1. During the initial transient regime, tracer flux changes in response to the evolving microstructure of mobile obstacles. Both microstructure and tracer flux eventually reach steady state after 2×10^9 Monte Carlo steps per lattice site.

Crowder aggregates show a variety of shapes as discussed above; at higher crowder density they tend to elongate in the direction parallel to the tracer gradient. Once the crowder clusters reach the sink they flatten against the surface. At long times, the sink may become fully covered with crowders. Thermal fluctuations may allow intermittent tracer diffusion through the surface layer of crowders. However, if the system becomes filled with tracers entirely, with no remaining vacancies, tracer diffusion drops to zero and the system remains permanently arrested.

Fig. 2 shows an overview of the configurations of the system for a range of crowder

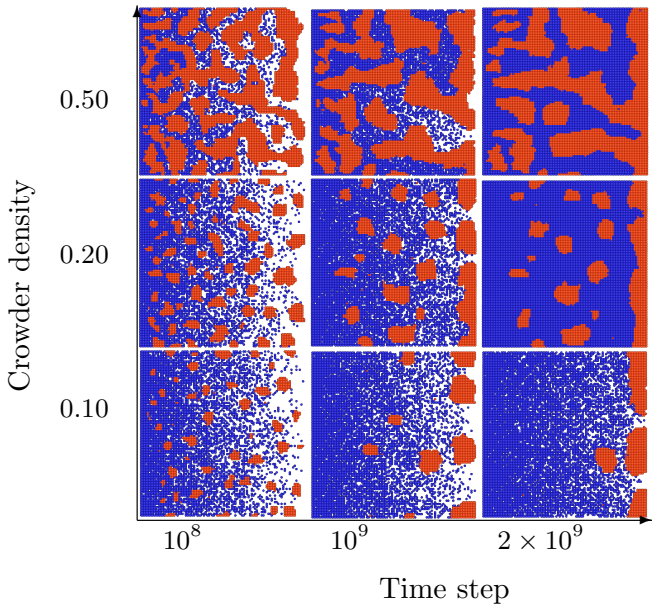

FIG. 1. Simulated temporal evolution showing diffusion and pattern formation for $k_{\mathrm{B}}T_{\mathrm{s}}/J_{\mathrm{int}} = 0.25$ at three distinct crowder densities: top row: $\rho_{\mathrm{C}} = 0.50$; middle row: $\rho_{\mathrm{C}} = 0.20$; bottom row: $\rho_{\mathrm{C}} = 0.10$, after 10^8 steps (left column), 10^9 steps (middle column), and 2×10^9 steps (right column). Crowders are shown in red and tracers in black, with a tracer source on the left side and tracer sink on the right side of the system. The two higher density systems have both arrested with the sink entirely blocked by crowders. The lower density system (bottom row) has not arrested but may do so at longer time scales. Movies showing time evolution of all three systems are included in Supplementary Information [53].

densities and temperatures, after 2×10^9 Monte Carlo steps per lattice site. Pattern formation depends sensitively on both crowder density and temperature. We focus on the interesting regimes of the phase space defined by crowder density, ρ_{C}, and temperature, T_{s}, to gain insight into the resulting microstructure and pattern formation.

At low temperature and low crowder density, crowders form small aggregates that do not move much or coarsen on the time scale of the simulation. The resulting microstructure represents a long-lived metastable state, which is reminiscent of diffusion through fixed obstables [55]. At low temperature and high crowder density, crowders quickly aggregate to form a maze-like metastable microstructure via spinodal decomposition [56, 57], through which tracer particles diffuse. At high enough crowder density, the crowder aggregates percolate and block tracer transport entirely. Diffusivity near the threshold density for

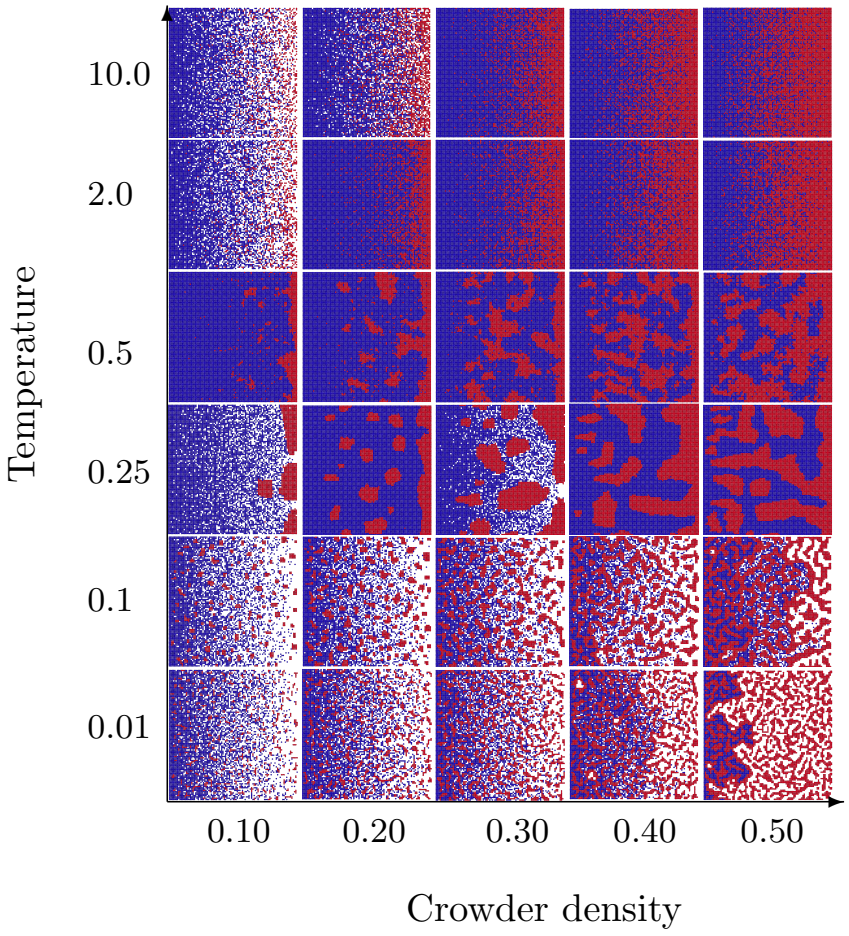

FIG. 2. Final configurations for varying values of crowder density and temperature. The x-axis represents crowder density (ρ_C) and the y-axis represents scaled temperature ($k_B T_s/J_{int}$). Tracers are shown in black and crowders are shown in red.

crowder percolation shows scaling behavior as discussed below.

At low-intermediate temperatures, $k_B T_s/J_{int} = 0.25$, we observe an intriguing transient behavior. Crowder aggregates form, coarsen, drift toward the sink, and flatten there. Observed morphologies also include formation of elongated structures parallel to the direction of tracer flow. At high-intermediate temperatures, $k_B T_s/J_{int} = 0.5$, all crowders drift immediately to the sink and aggregate there, and tracer diffusion is blocked entirely.

At high temperatures, $k_B T_s/J_{int} \geq 1.0$, for low crowder density, crowders aggregate to form a layer covering the sink but remain sufficiently disordered to allow non-zero tracer diffusion. At high crowder density, tracer diffusion is fully-blocked.

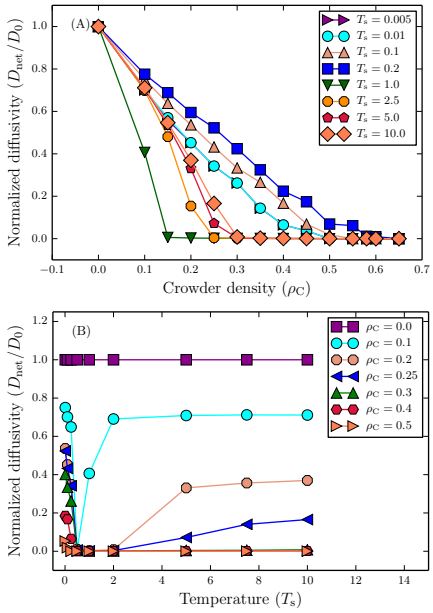

FIG. 3. Normalized diffusivity as a function of (A) crowder density (ρ_C) at fixed simulation temperatures (T_s), and as a function of (B) simulation temperature (T_s) at fixed crowder densities (ρ_C). Legends show the fixed values of temperatures and crowder densities, respectively. Net tracer flux is computed by counting the rate of tracers annihilating at the sink per unit length per unit time. We define the net diffusivity of tracers as D_{net}, and define D_0 as the net diffusivity of tracers in the absence of crowders. The quantity D_{net}/D_0 is thus calculated as tracer flux (with crowders) normalized by the tracer flux in the absence of crowders.

Dependence of diffusivity on crowder density and temperature

Tracer diffusivity as a function of crowder density and temperature is shown in Fig. 3. For crowder density below 0.3, we observe re-entrant behavior, as tracer diffusivity first drops to zero and then rises with increasing temperature. Diffusivity as a function of crowder density also shows complex, non-monotonic behavior.

To gain insight into these results, we consider various limits where analytic predictions are possible.

High temperature limit: analytic solution

In the limit of very high temperature ($k_B T_s/J_{int} \to \infty$), equivalent to $J_{int} \to 0$, crowders have only excluded volume interactions. In this case, tracers and crowders are chemically

equivalent except for their distinct boundary conditions, and the system is equivalent to a random walk model with two types of particles, where the tracer species has a source and a sink, and the number of crowders is fixed. In this high temperature limit, we note that our model is equivalent to the work of Simpson et al [58], who studied a lattice-based random walk model with two or more mobile species with the same diffusivity and only excluded volume interactions. The setup of their model consists of partitioning the population of a single species into subpopulations with identical diffusivity. In this limit, where tracers and crowders are chemically equivalent, there is no phase separation and we can solve the diffusion equation analytically. The diffusion equation for this scenario can be written as

$$\frac{\partial(T(x)+C(x))}{\partial t} = D\Big(\frac{\partial^2(T(x)+C(x))}{\partial x^2}\Big) \tag{1}$$

where, $T(x)$ and $C(x)$ represent the tracer and crowder density profiles, position x goes from 0 (source) to L (sink), and D represents the self-diffusion coefficient of both species. To find the steady-state solution of the diffusion equation, as an ansatz we consider a solution of the form

$$T(x) = a_0 + a_1 x + a_2 x^2 \tag{2}$$

$$C(x) = b_0 + b_1 x + b_2 x^2 \tag{3}$$

and apply the boundary conditions $T(x=0)=1$, $T(x=L)=0$, and $\frac{1}{L}\int_0^L C(x)dx = \rho_{\mathrm{C}}$ to find the coefficients $\{a_i, b_i\}$.

The resulting steady-state solution in the high temperature limit is

$$T(x) = 1 - (1-3\,\rho_{\mathrm{C}})\frac{x}{L} - (3\,\rho_{\mathrm{C}})\frac{x^2}{L^2} \tag{4}$$

$$C(x) = (3\,\rho_{\mathrm{C}})\frac{x^2}{L^2} \tag{5}$$

Fig. 4 compares this analytical result with Monte Carlo simulation data in the case $J_{\mathrm{int}} = 0$, showing time-averaged density profiles for tracer and crowder species; analytical and simulation results are in good agreement. Density profiles $T(x)$ and $C(x)$ for tracer and crowder species, respectively, were calculated by averaging over the y direction; time averaged over the last 10% of each simulation to capture the steady state behavior; and averaged over 10 independent simulations, each lasting at least 2×10^9 Monte Carlo steps.

This result shows that even without attractive interactions, crowder density is depleted near the tracer source and concentrated near the tracer sink.

Resulting steady state flux of particles of both types is calculated as $J = -D\frac{d(T(x)+C(x))}{dx} = D(1-3\,\rho_{\mathrm{C}})$. Here, D is the self-diffusion coefficient of both tracers and crowders. Since crowders cannot exit the simulation box, this flux represents the net flow of tracers. Thus in the high temperature limit, tracer flux, and thus net diffusivity, is proportional to $(1-3\,\rho_{\mathrm{C}})$. Hence, tracer flux vanishes entirely for crowder density $\rho_{\mathrm{C}} \geq 1/3$. At such high crowder density, after an initial transient, the sink is blocked entirely by crowders and tracer flux drops to zero. This result is verified via Monte Carlo simulation as shown in Fig. 4(B). Here, net diffusivity of tracers is calculated by counting the flux of tracers exiting at the sink, per unit length and time, averaged over ten independent simulations, excluding the initial transient before the systems have reached steady state. This quantity is normalized by the flux in the absence of crowders. We note that in a related model of diffusion in crowded environments, Ellery et al [15] also found threshold behavior with obstacle density around 0.3; but as their system has immobile obstacles, this threshold behavior is driven by a fundamentally different mechanism.

The good agreement of analytic solution and simulation data in the limit of $J_{\mathrm{int}} \to 0$ case is somewhat intriguing in the light of simple exclusion processes in non-equilibrium statistical mechanics [59–61]. Macroscopic transport principles concerning Eq. 1 provides an approximate description of two species competing for space [62–64]. Nevertheless, it is reasonable to describe the system evolution in terms of macroscopic transport equation when two species are chemically equivalent in the limit of high temperature.

Low temperature limit: scaling behavior near the percolation threshold

At low temperature, crowders quickly aggregate into clusters that are essentially immobile and do not drift toward the sink on the time scale observed in our simulations. At low crowder density, these clusters act as fixed obstacles and allow continuous tracer diffusion. At higher density, crowders aggregate into an extended network that entirely blocks tracer diffusion. Near the threshold density, we observe scaling behavior. Fig. 5 shows the dependence of tracer flux as a function of $(\rho_{\mathrm{C}} - \rho^{\star}_{\mathrm{C}})$ on a log-log plot, for $k_{\mathrm{B}}T_{\mathrm{s}}/J_{\mathrm{int}} = 0.1$.

Scaling behavior is observed for $\rho^{\star}_{\mathrm{C}} = 0.43$. The diffusive flux scales as $(\rho_{\mathrm{C}} - \rho^{\star}_{\mathrm{C}})^{\alpha}$ with

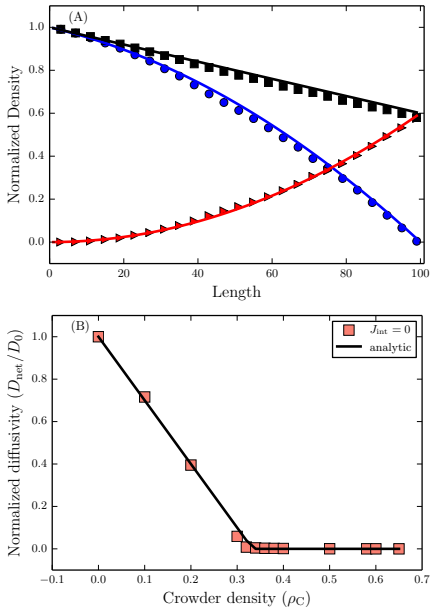

FIG. 4. (A) Density profiles of tracers (red triangles), crowders (black circles) and their sum (black squares) for the high temperature limit at a value of crowder density $\rho_{\rm C} = 0.2$. Solid line represent analytic solutions given by Eqs. 4 - 5 and their sum. (B) Normalized diffusivity as a function of crowder density for the scenario where the exchange coefficient of interaction, $J_{\rm int} = 0$. Squares represent simulated data points and the solid line represent analytic solution for diffusivity.

$\alpha \approx 4/3$. Interestingly, this value of the exponent is in good agreement with the scaling exponent for conductivity through a random resistor network model near its percolation threshold [65–67]. Fick's law in steady state for diffusion is equivalent to Kirchoff's law of conductivity through an electrical network. Hence, steady state diffusion of tracers around randomly distributed obstacles is related to the electrical conductivity of a random resistor network. This relationship has been previously noted and explained in the literature [68].

If the crowders were immobile and randomly distributed with no spatial correlations, tracer flux would show scaling behavior near the critical density where open sites form a percolating connected pathway between the source and the sink. As the percolation threshold, p_c, for the square site lattice is ≈ 0.59, we would expect scaling behavior near $\rho_{\rm C}^{\star} = 1 - p_c \approx 0.41$. Instead, we found scaling behavior near $\rho_{\rm C}^{\star} \approx 0.43$. The slight change in the percolation threshold is due to spatial correlations due to crowder interactions [69]. In the low temperature limit, near the percolation threshold, random walks on a fractal should produce anomalous diffusion [70]. By analogy with the random resistor network, we can

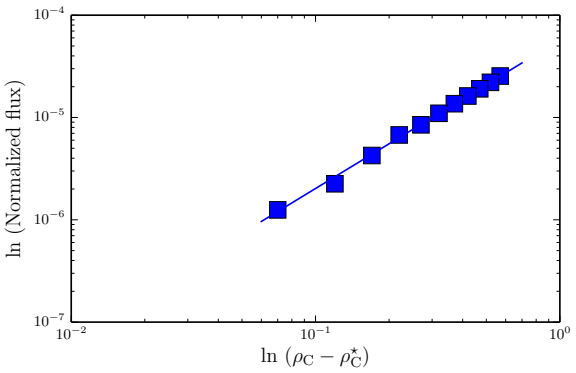

FIG. 5. Time-averaged tracer flux as a function of $(\rho_C - \rho_C^\star)$ at a temperature corresponding to $k_B T_s / J_{int} = 0.1$. Squares represent simulation data and the solid line is a linear fit to the simulated data with scaling exponent $\alpha \approx 4/3$.

expect diffusive flux to scale as $(\rho_C - \rho_C^\star)^\alpha L^{d-2}$ [71], where L is the system size. Thus, in two dimensions, near the percolation threshold, we do not expect the diffusivity to scale in an interesting way with the system size.

DISCUSSION

Although the model described here is remarkably simple, the interaction of phase separation with gradient-driven diffusion is nevertheless complex. The dependence of diffusive tracer flux can be summarized by a single function of crowder density and temperature only in the high temperature limit $k_B T_s / J_{int} \to \infty$, where no phase separation occurs. The resulting diffusivity in the high temperature limit is

$$\left.\begin{aligned} D_{net} &= D_0(1 - 3\rho_C) \;\; ; \;\; \rho_C < 1/3 \\ &= 0 \;\; ; \;\; \rho_C \geq 1/3 \end{aligned}\right\}, \tag{6}$$

where, D_0 is the diffusivity in the absence of any crowders in the system.

In the limit of low temperature near the percolation transition, the system shows scaling behavior where we find the following dependence of diffusivity on crowder density:

$$\left.\begin{aligned} D_{net} &= D_0 \left(\rho_C - \rho_C^\star\right)^{4/3} \;\; ; \;\; \rho_C < \rho_C^\star \\ &= 0 \;\; ; \;\; \rho_C \geq \rho_C^\star \end{aligned}\right\}, \tag{7}$$

where, $\rho_C^\star = 1 - p_c = 0.43$, is the critical crowder density above which tracer diffusivity drops to zero.

When a multi-component mixture phase separates in the presence of gradient-driven diffusion, the resulting tracer flux depends on the evolving microstructure and in turn influences microstructural evolution. Although the multi-species lattice gas model presented in this work is highly idealized, it demonstrates this key mechanism. Intracellular transport in complex biological media involves more complex interactions than a lattice gas model can represent. In a recent study involving diffusive motion of particles in an environment of spherical crowders, a non-monotonic dependence of the diffusion rate on the strength of crowder-diffuser attraction was observed [72]. Relevant experimental studies also include diffusion in a lipid mixture monolayer at the air-water interface [51], such as in a Langmuir trough [73], where lipid raft formation, may for instance, inhibit gradient-driven diffusion of other molecular species. In the simplified and highly idealized model presented in this paper, we assume that isolated "tracers" and "crowders" have the same radius and self-diffusion coefficient. In experimental systems, two chemical species may of course have completely different properties. Likewise, we have neglected the possibility of attractive or repulsive interactions between tracers and crowders, and the potential role of hydrodynamic interactions, that is, the scenario in an off-lattice model. We plan to address these interesting avenues in future work.

ACKNOWLEDGMENTS

The authors gratefully acknowledge financial support from the National Science Foundation grant DMR-1409658.

---

[1] W. M. Gelbart and A. Ben-Shaul, The Journal of Physical Chemistry **100**, 13169 (1996).

[2] B. Schmittmann and R. Zia, Physics Reports **301**, 45 (1998).

[3] G. F.-L. Ames, Annual Review of Biochemistry **55**, 397 (1986).

[4] S. B. Zimmerman and A. P. Minton, Annual Review of Biophysics and Biomolecular Structure **22**, 27 (1993).

[5] J. C. Skou, Physiol. Rev **45**, 617 (1965).

[6] K. Simons and E. Ikonen, Nature **387**, 569 (1997).

[7] J. A. Dix and A. Verkman, Annu. Rev. Biophys. **37**, 247 (2008).

[8] B. P. English, V. Hauryliuk, A. Sanamrad, S. Tankov, N. H. Dekker, and J. Elf, Proc. Natl. Acad. Sci. U. S. A. **108**, E365 (2011).

[9] M. Długosz and J. Trylska, BMC Biophysics **4**, 3 (2011).

[10] I. Golding and E. C. Cox, Phys. Rev. Lett. **96**, 098102 (2006).

[11] S. C. Weber, A. J. Spakowitz, and J. A. Theriot, Phys. Rev. Lett. **104**, 238102 (2010).

[12] M. J. Saxton, Biophys J. **58**, 1303 (1990).

[13] H. Berry and H. Chaté, arXiv preprint arXiv:1103.2206 , 1 (2011).

[14] A. J. Ellery, M. J. Simpson, S. W. McCue, and R. E. Baker, J. Chem. Phys. **140**, 054108 (2014).

[15] A. J. Ellery, R. E. Baker, and M. J. Simpson, Physical Biology **13**, 05LT02 (2016).

[16] P. A. Fedders and O. Sankey, Phys. Rev. B **18**, 5938 (1978).

[17] K. Nakazato and K. Kitahara, Progress of Theoretical Physics **64**, 2261 (1980).

[18] K. Kehr, R. Kutner, and K. Binder, Phys. Rev. B **23**, 4931 (1981).

[19] R. Kutner, K. Binder, and K. Kehr, Phys. Rev. B **26**, 2967 (1982).

[20] R. Tahir-Kheli and R. Elliott, Phys. Rev. B **27**, 844 (1983).

[21] R. Kutner and K. Kehr, Philosophical Magazine A **48**, 199 (1983).

[22] R. Kutner, K. Binder, and K. Kehr, Phys. Rev. B **28**, 1846 (1983).

[23] K. Kehr, Journal of Statistical Physics **30**, 509 (1983).

[24] M. Schoen and C. Hoheisel, Molecular Physics **52**, 33 (1984).

[25] R. Kutner, Journal of Physics C: Solid State Physics **18**, 6323 (1985).

[26] R. Granek and A. Nitzan, J. Chem. Phys. **92**, 1329 (1990).

[27] R. Granek and A. Nitzan, J. Chem. Phys. **93**, 5918 (1990).

[28] D. H. Rothman and S. Zaleski, Rev. Mod. Phys. **66**, 1417 (1994).

[29] D. Brown and E. London, Annual Review of Cell and Developmental Biology **14**, 111 (1998).

[30] R. Vasanthi, S. Bhattacharyya, and B. Bagchi, J. Chem. Phys. **116**, 1092 (2002).

[31] M. Vrljic, S. Y. Nishimura, S. Brasselet, W. Moerner, and H. M. McConnell, Biophys. J. **83**, 2681 (2002).

[32] J.-H. Jeon, V. Tejedor, S. Burov, E. Barkai, C. Selhuber-Unkel, K. Berg-Sørensen, L. Oddershede, and R. Metzler, Phys. Rev. Lett. **106**, 048103 (2011).

[33] A. Zaccone and E. M. Terentjev, Phys. Rev. E **85**, 061202 (2012).

[34] I. M. Sokolov, Soft Matter **8**, 9043 (2012).

[35] J.-H. Jeon, M. Javanainen, H. Martinez-Seara, R. Metzler, and I. Vattulainen, Phys. Rev. X **6**, 021006 (2016).

[36] S. K. Ghosh, A. G. Cherstvy, D. S. Grebenkov, and R. Metzler, New Journal of Physics **18**, 013027 (2016).

[37] M. J. Saxton, Biophys J. **52**, 989 (1987).

[38] M. J. Saxton, Biophys J. **64**, 1053 (1993).

[39] M. J. Saxton, Biophys J. **66**, 394 (1994).

[40] M. J. Saxton, Biophys J. **70**, 1250 (1996).

[41] M. J. Saxton, Biophys J. **92**, 1178 (2007).

[42] C. Echeveria, K. Tucci, and R. Kapral, J. Phys. Condens. Matter. **19**, 065146 (2007).

[43] M. J. Saxton, Biophys J. **94**, 760 (2008).

[44] E. Vilaseca, A. Isvoran, S. Madurga, I. Pastor, J. L. Garcés, and F. Mas, Phys Chem Chem Phys **13**, 7396 (2011).

[45] J. Schöneberg, A. Ullrich, and F. Noé, BMC Biophysics **7**, 1 (2014).

[46] T. Ando and J. Skolnick, Proc. Nat. Acad. Sci. U. S. A. **107**, 18457 (2010).

[47] S. K. Ghosh, A. G. Cherstvy, and R. Metzler, Phys Chem Chem Phys **17**, 1847 (2015).

[48] H. Berry and H. Chaté, Phys. Rev. E **89**, 022708 (2014).

[49] J. D. Schmit, E. Kamber, and J. Kondev, Phys. Rev. Lett. **102**, 218302 (2009).

[50] H. Kang, P. A. Pincus, C. Hyeon, and D. Thirumalai, Phys. Rev. Lett. **114**, 068303 (2015).

[51] B. M. Neumann, D. Kenney, Q. Wen, and A. Gericke, Biophys. J. **3**, 576a (2016).

[52] N. Metropolis, A. W. Rosenbluth, M. N. Rosenbluth, A. H. Teller, and E. Teller, J. Chem. Phys. **21**, 1087 (1953).

[53] *See Supplemental Material at [URL will be inserted by publisher] for movies showing temporal evolution of the three systems shown in Fig. 1, all at temperature* $T_s = 0.25$*, for different values of the crowder density* ρ_C*. Movie 1 shows* $\rho_C = 0.1$*; Movie 2 shows* $\rho_C = 0.2$*; and Movie 3 shows* $\rho_C = 0.5$*.*

[54] R. B. Selinger and H. E. Stanley, Phys. Rev. A **42**, 4845 (1990).

[55] D. V. Nicolau, J. F. Hancock, and K. Burrage, Biophys. J. **92**, 1975 (2007).

[56] J. W. Cahn, Acta Metallurgica **9**, 795 (1961).

[57] R. Ball and R. Essery, Journal of Physics: Condensed Matter **2**, 10303 (1990).

[58] M. J. Simpson, K. A. Landman, and B. D. Hughes, Physica A: Statistical Mechanics and its

Applications **388**, 399 (2009).

[59] P. M. Richards, Phy. Rev. B **16**, 1393 (1977).

[60] V. Privman, *Nonequilibrium statistical mechanics in one dimension* (Cambridge University Press, 2005).

[61] T. M. Liggett, *Stochastic interacting systems: contact, voter and exclusion processes*, Vol. 324 (Springer Science & Business Media, 2013).

[62] D. Fanelli and A. J. McKane, Phys. Rev. E **82**, 021113 (2010).

[63] D. Fanelli, A. McKane, G. Pompili, B. Tiribilli, M. Vassalli, and T. Biancalani, Physical Biology **10**, 045008 (2013).

[64] M. Galanti, D. Fanelli, A. Maritan, and F. Piazza, EPL (Europhysics Letters) **107**, 20006 (2014).

[65] R. Fisch and A. B. Harris, Phys. Rev. B **18**, 416 (1978).

[66] B. Derrida, D. Stauffer, H. Herrmann, and J. Vannimenus, Journal de Physique Lettres **44**, 701 (1983).

[67] C. Pennetta, G. Trefán, and L. Reggiani, Phys. Rev. Lett. **85**, 5238 (2000).

[68] F. Höfling and T. Franosch, Reports on Progress in Physics **76**, 046602 (2013).

[69] R. Blumberg, G. Shlifer, and H. E. Stanley, Journal of Physics A: Mathematical and General **13**, L147 (1980).

[70] S. Havlin and D. Ben-Avraham, Advances in Physics **51**, 187 (2002).

[71] S. Redner, in *Mathematics of Complexity and Dynamical Systems* (Springer, 2012) pp. 446–462.

[72] G. G. Putzel, M. Tagliazucchi, and I. Szleifer, Phys. Rev. Lett. **113**, 138302 (2014).

[73] M. Gudmand, M. Fidorra, T. Bjørnholm, and T. Heimburg, Biophys. J. **96**, 4598 (2009).